Cross-section measurements for the ^{57}Fe(n,nγ)^{57}Fe and ^{57}Fe(n,2nγ)^{56}Fe reactions

A. Negret, M. Sin, C. Borcea, R. Capote, Ph. Dessagne, M. Kerveno, N. Nankov, A. Olacel, A. J. M. Plompen, and C. Rouki

Phys. Rev. C **96**, 024620 — Published 23 August 2017

DOI: 10.1103/PhysRevC.96.024620

Cross-section measurements for the ^{57}Fe(n, $n\gamma$)^{57}Fe and ^{57}Fe(n, $2n\gamma$)^{56}Fe reactions

A. Negret,[1,*] M. Sin,[2] C. Borcea,[1] R. Capote,[3] Ph. Dessagne,[4]
M. Kerveno,[4] N. Nankov,[5] A. Olacel,[1] A.J.M. Plompen,[5] and C. Rouki[5]

[1]*Horia Hulubei National Institute for Physics and Nuclear Engineering, 077125 Bucharest-Măgurele, Romania*
[2]*University of Bucharest, Faculty of Physics, 077125 Bucharest-Măgurele, Romania*
[3]*Nuclear Data Section, International Atomic Energy Agency, Vienna A-1400, Austria*
[4]*Université de Strasbourg, CNRS, IPHC UMR7178, F-67000 Strasbourg, France*
[5]*European Commission, Joint Research Centre - Geel, B-2440 Geel, Belgium*

(Dated: July 31, 2017)

A neutron inelastic scattering experiment was performed on an enriched ^{57}Fe sample at the GELINA (Geel Electron Linear Accelerator) neutron source using the GAINS (Gamma Array for Neutron Inelastic Scattering) spectrometer. Several γ-production cross sections were determined, but the first transition (14.4 keV) could not be detected due to the steadily increased γ background at low energies. Consequently we use an interplay between experimental data and carefully tuned theoretical calculations to generate the total inelastic cross section.

PACS numbers: 25.40.Fq, 29.30.Kv, 27.40.+z

I. INTRODUCTION

Iron is undoubtedly a key structural material for the development of any nuclear facility. The Collaborative International Evaluated Library Organization Pilot Project (CIELO), a subgroup of the Working Party on International Nuclear Data Evaluation Co-operation (WPEC) of the Nuclear Energy Agency [1] focuses on the evaluation of the most abundant isotope, ^{56}Fe, while an entry of the High Priority Request List (HPRL) [2] hosted by the same agency is dedicated specifically to the neutron inelastic scattering measurements on ^{56}Fe. Having recently published an article describing a high precision cross section measurement of the ^{56}Fe(n, n') reaction [3], we report now on an experiment on the minor isotope ^{57}Fe.

Four stable iron isotopes exist, with the following natural abundances: ^{54}Fe - 5.85(11)%, ^{56}Fe - 91.75(11)%, ^{57}Fe - 2.12(3)%, and ^{58}Fe - 0.28(1)% [4]. The fist excited level in the major isotope ^{56}Fe is at 846.8 keV [5] and therefore, at energies lower than 861 keV neutron moderation can occur in ^{nat}Fe only through elastic scattering (much less effective) or through inelastic scattering on the minor isotopes. ^{57}Fe has 4 excited levels below 861 keV [6] while ^{54}Fe has none [7]. Moreover, the neutron moderation through inelastic scattering on ^{57}Fe produce γ radiation that has to be taken into account in the energy balance of the reactors.

The current experiment was particularly challenging due to two major difficulties. First, the availability of sufficient enriched iron was a serious issue. Second, the energy of the first excited level in ^{57}Fe is as low as 14.4 keV [6] and the γ decay from this state could not be observed with our experimental setup. Both experimental limitations will be discussed in detail.

*Email: alnegret@tandem.nipne.ro

A previous measurement performed at the Oak Ridge Electron Linear Accelerator (ORELA) operated by Oak Ridge National Laboratory (ORNL) is reported in Ref. [8]. The authors used a 22.19-m flight path and one Ge(Li) detector placed at 125° with regard to the incoming neutron beam and measured a significant number of γ-production cross sections from the (n, n'), (n, $2n$) and (n, α) channels. We will compare our results with the cross sections reported in Ref. [8].

The present article is organized as follows: after a short overview of the experimental setup, Section III emphasizes the particularities of this measurement. Section IV shortly reviews several theoretical aspects and Section V discusses extensively the experimental results.

II. EXPERIMENTAL SETUP

The experimental setup is very similar to the one used in several previous measurements [9–11]. It consists of the neutron source GELINA (Geel Electron Linear Accelerator) [12], the HPGe array GAINS (Gamma Array for Inelastic Neutron Scattering) [13] and a ^{235}U fission chamber [14] used for data normalization.

The neutron source GELINA operated by the Joint Research Centre of the European Commission in Geel, Belgium is a linear accelerator shooting high-intensity electron pulses on a rotating depleted uranium target. A compression magnet allows the reduction of the pulse length to about 1 ns, thus defining the unique time resolution of the facility [15]. Following bremsstrahlung and (γ, n) reactions, neutrons are produced together with a very intense γ flash. The neutron flux is significant for energies ranging from ≈70 keV to ≈18 MeV. During the present measurement GELINA was operated at a repetition rate of 800 Hz.

The GAINS array was centered around the ^{57}Fe sample located at the end of an 198.684-m flight path. Although the setup can accommodate up to 12 HPGe detectors (see

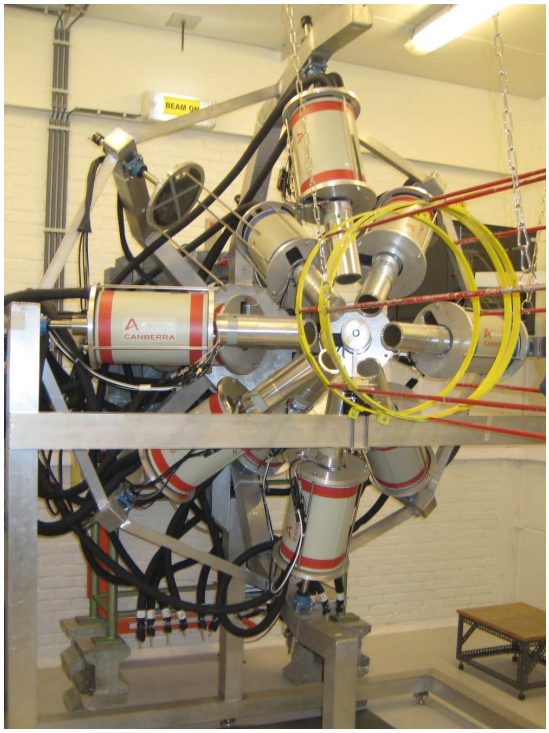

FIG. 1: (Color online) Gamma Array for Inelastic Neutron Scattering (GAINS), the HPGe-based spectrometer used in the current experiment.

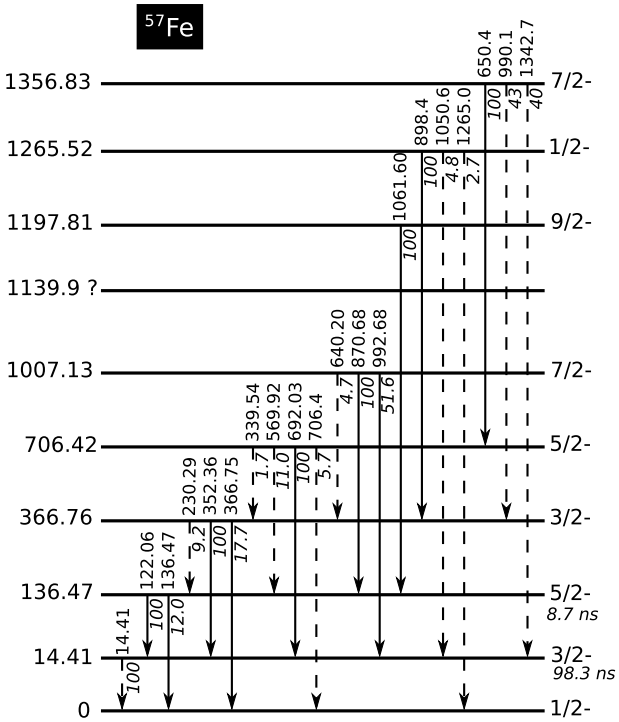

FIG. 2: Low excitation energy level scheme of ^{57}Fe according to Ref. [6]. γ-production cross sections were determined for the transitions drawn with continuous lines.

Fig. 1), only 6 HPGe detectors placed at 110° and 150° with regard to the incoming neutron beam were used in the current data analysis. This choice of angles specific to GAINS allows an optimal integration of the angular distribution of the γ rays using a Gauss quadrature as described in Ref. [16].

At the sample position the neutron beam was collimated to a diameter of 61 mm. The enriched iron sample was larger than the beam and had an effective areal density of 0.491(5) g/cm^2 (i.e. a thickness of about 0.67 mm). It contained 90.50(30)% ^{57}Fe, 9.15(30)% ^{56}Fe, 0.25(2)% ^{54}Fe, and 0.10(1)% ^{58}Fe. The sample did not have a uniform shape and it presented rounded edges. Therefore, in calculating the effective areal density of the portion of the sample that was exposed to the neutron flux we assumed that this region was 3(1)% thicker than the average areal density obtained by weighting the sample and measuring its area. All cross section values calculated in the current work took into account the isotopic content and the shape of the sample and the reported values correspond to pure ^{57}Fe.

We note that the sample procurement was one of the key issues of the current experiment, as the price of such quantity of ^{57}Fe-enriched iron is not negligible. It was provided by the Isotope Office of the Oak Ridge National Laboratory.

The neutron flux was monitored using a ^{235}U fission chamber placed at a distance of 197.214 m from the neutron source, about 1.5 m before the sample. The total thickness of the ^{235}U layers is 3.0896(1) mg/cm^2 and their diameter (≈70 mm) is larger than the beam. All corrections discussed in Ref. [14] were properly applied to the neutron flux calculation. The standard ^{235}U(n, f) cross section [17] was used to normalize our results.

III. EXPERIMENTAL PARTICULARITIES

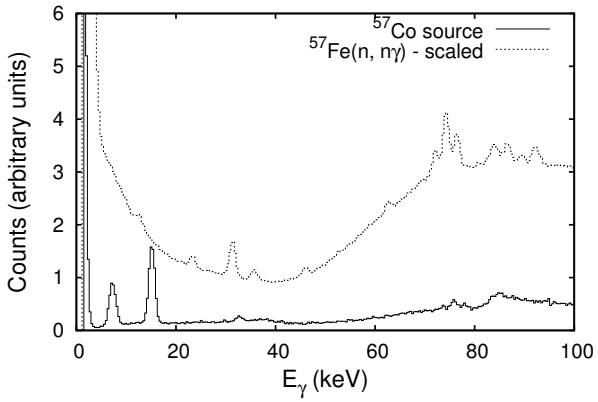

FIG. 3: Background level in γ spectra around 14 keV.

As briefly mentioned in the introduction, besides the availability of the enriched sample, the main difficulty

of the current experiment was related to the particular structure of the ^{57}Fe nucleus. The low excitation energy region of the evaluated level scheme from Ref. [6] is displayed in Fig. 2. Continuous lines represent transitions that were measured in the current experiment and for which we built the γ-production cross sections. As shown in Fig. 2, the first excited level in ^{57}Fe lies at 14.4 keV and the decaying transition, having a conversion coefficient of 8.56(26), could not be detected (see below). Moreover, the half-life of this level is 98.3 ns, partially decorrelating the time of the reaction from the 14.4-keV γ emission.

Fig. 3 displays the low energy region of two γ spectra recorded by one of our detectors. The continuous line shows the spectrum from a ^{57}Co source while the dotted line represents the scaled spectrum recorded online from the ^{57}Fe(n, $n\gamma$) reaction. The ^{57}Co source populates through electron capture decay the excited levels in ^{57}Fe and therefore the γ lines are the same as those from the inelastic scattering of neutrons on ^{57}Fe. We carefully tuned the data acquisition electronics lowering all thresholds as much as possible and indeed, on the spectrum acquired from the ^{57}Co source the 14.4-keV transition is clearly visible together with a 7-keV X ray. Nevertheless, those peaks are completely covered by the background in the ^{57}Fe(n, $n\gamma$) spectrum.

Most probably, the steady background increase at very low γ energy in our (n, $n\gamma$) spectra is caused by the neutrons scattered on the sample or in the air that interact elastically with germanium nuclei from the crystals of our detectors. Following such an interaction the recoil energy of the Ge nucleus is deposited inside the crystal and detected as a low-amplitude signal. This neutron-induced background, correlated in time with the neutron pulses, prevents the detection of the low energy γ rays of interest. We also note that the absorption coefficient of the 14.4-keV γ rays in iron is very high and therefore this radiation was strongly absorbed in the sample: such low-energy photons could penetrate only through a very thin layer of 20-30 μm while the rest of the target did not contribute. Consequently we were not able to build the γ-production cross section for the 14.4-keV transition.

IV. THEORETICAL CONSIDERATIONS

Considering the experimental limitations described in the previous section, a theoretical support is required not only to validate but also to complete our measurements in order to predict the total inelastic cross section for the ^{57}Fe(n, n') reaction. For this purpose, two well known model codes have been employed - EMPIRE-3.2 (MALTA) [18, 19] and TALYS 1.8 [20]. Both codes are used worldwide for nuclear reaction studies and for nuclear data evaluation. They are well maintained and benefit from constantly updated reaction models. Model parameters are retrieved from RIPL-3 (Reference Input Parameter Library) [21] and from the internal systematics. Being used in nuclear data evaluations, these model codes have the tools to compensate the deficiencies of models and parameters preserving the consistency of the calculations.

In TALYS and EMPIRE the cross section of γ emission in a transition between an initial discrete level L_i and a final level L_f ($\sigma_{n,n'_i\gamma_{i,f}}$), is calculated as the product of the population cross section of the level L_i (σ_{n,n'_i}) and the branching ratio of the γ ray emitted in the $L_i \rightarrow L_f$ transition ($b_{\gamma_{i,f}}$). The population cross sections are obtained using nuclear reaction models while the branching ratios are mainly the results of experimental studies on the nuclear structure

$$\sigma_{n,n'_i\gamma_{i,f}} = \sigma_{n,n'_i} b_{\gamma_{i,f}}. \quad (1)$$

In a nuclear reaction, there are two contributions to the population of a discrete excited level: one coming directly from the reaction (the so-called side-feeding) and the other coming from the γ cascade from the levels above, situated in the discrete or in the continuum region. In a process such as (n, $n\gamma$), three reaction mechanisms can contribute to the side feeding of the residual nucleus in a discrete excited level: the direct interaction (σ^{DI}_{n,n'_i}), the preequilibrium emission (σ^{PE}_{n,n'_i}) and the compound nucleus formation (σ^{CN}_{n,n'_i}). The calculation of the γ-transition cross sections from the continuum to the discrete region $\sigma_{n,n_c\gamma_{c,i}}$ uses level densities and γ-strength functions provided by closed formulas or by microscopic predictions. Adding all these contributions, the population cross section of a discrete excited level reads

$$\sigma_{n,n'_i} = \sigma^{DI}_{n,n'_i} + \sigma^{PE}_{n,n'_i} + \sigma^{CN}_{n,n'_i} + \sum_{h>i}^{N_d} \sigma_{n,n'_h} b_{\gamma_{h,i}} + \sigma_{n,n_c\gamma_{c,i}}, \quad (2)$$

where N_d is the number of discrete levels considered in the calculation. The continuum starts just above level N_d.

Note that this expression neglects the effect of nuclear deformation on the calculated σ^{CN}_{n,n'_i} cross section. Such effects have been discussed in Refs. [22, 23], and are expected to be very small for an odd-even iron nucleus like ^{57}Fe. Equations (1) and (2) show that the (n, $n\gamma$) cross sections are sensitive to three different reaction models and parameters, but also to the target nuclear structure and level scheme. Consequently, the description of these experimental cross sections is a very challenging test for the reaction model codes.

In the case of iron isotopes, the theoretical prediction is particularly difficult because large fluctuations in the total cross section were experimentally observed up to almost 5-6 MeV incident energy. Similar fluctuations appeared in our ^{56}Fe(n, $n\gamma$) measurement [3], and were also reported in the high-resolution elastic measurements by Kinney and McConnell [24]. Statistical codes such as TALYS and EMPIRE are based on the optical model which

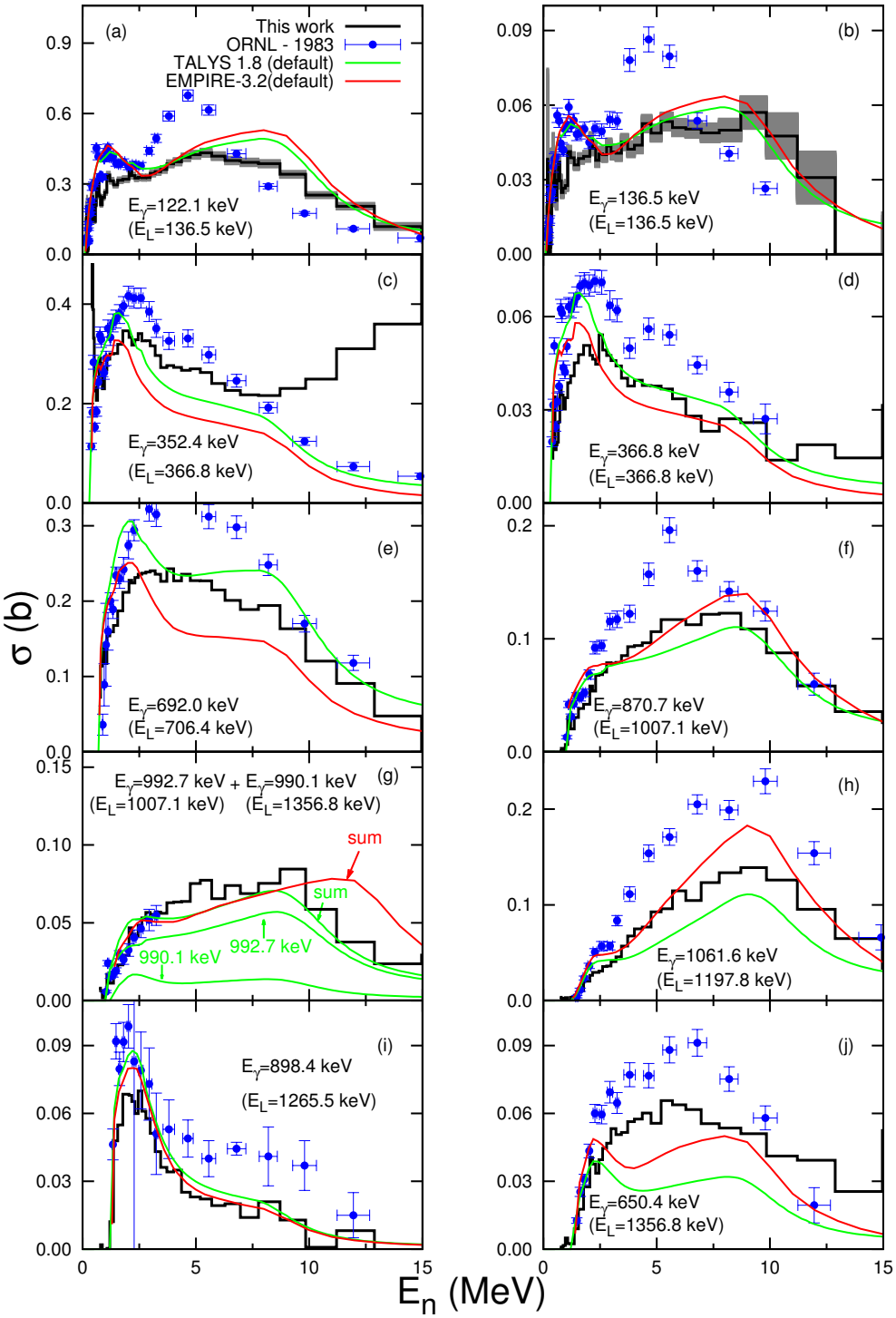

FIG. 4: (Color online) Production cross sections for the γ rays emitted following the ^{57}Fe(n, $n\gamma$) reaction. The gray bands from panels (a) and (b) represent total uncertainty limits. Data are compared with the results of a previous measurement [8] and with TALYS and EMPIRE calculations using default parameters.

can only describe an average of these resonance structures. Additionally, the customary coupled-channel optical model applied to iron isotopes faced problems related to the nuclear structure of these nuclei (e.g., the averaged measured total cross sections on ^{56}Fe is about ≈1 b, which is about 30-40% lower than the value calculated using a typical optical model). These aspects are confirmed by the present calculations (as will be shown in Section V) and by other ongoing studies within the CIELO project [1, 25, 26].

V. RESULTS AND DISCUSSIONS

The primary results of our experiment are the γ-production cross sections. After identifying in our measured spectra the peaks corresponding to transitions in ^{57}Fe and after selecting only those transitions that seem to be less affected by background we built the production cross section for 10 γ rays. These are represented by black lines in Fig. 2. The γ-production cross section of the 846.8-keV transition excited in the ^{57}Fe(n, $2n$) reaction was deduced by corroborating the current data with those from a previous measurement [3]. Further, we built the 136.5-, 366.8- and 706.4-keV level cross sections based on their population and decay patterns. Finally, we employed the reaction code EMPIRE to deduce the total inelastic cross section.

A. ^{57}Fe(n, n')^{57}Fe γ-production cross sections

1. *Experimental results*

Figure 4 displays the γ-production cross sections for 10 transitions decaying from 7 levels with excitation energies between 136.5 and 1356.8 keV. Our results are compared with previous data reported in Ref. [8] but also with default TALYS and EMPIRE calculations mentioned above.

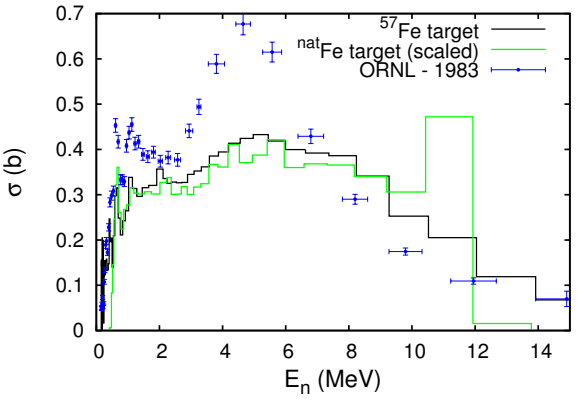

FIG. 5: (Color online) Production cross sections for the 122.1-keV γ ray: comparison of the results obtained using the present ^{57}Fe-enriched sample (black line), the one obtained in a previous experiment using a ^{nat}Fe target (green line) [3] and the result from Ref. [8] (blue dots). The cross sections obtained with the ^{nat}Fe target are only relative values.

In order to reduce the statistical uncertainties we grouped several time bins thus sacrificing the neutron energy resolution. Nevertheless, the number of points displayed for each γ-production cross section remains high compared to the previous measurement.

Significant differences exist between our results and the previous measurement performed at ORNL. The decay of the second excited level in ^{57}Fe (E$_L$=136.5 keV, $J^\pi = 5/2^-$) occurs through a strong γ transition of 122.1 keV and a much weaker γ ray of 136.5 keV. The ORNL measurement [see Fig. 4(a) and (b)] shows in both cases double-humped shapes for the γ-production cross sections suggesting a strong population of the level at small neutron energies and then an even stronger population in the quasi-continuum region. On the contrary, our cross sections increase almost continuously with neutron energy up to E$_n$ ≈10 MeV. We note that, above this energy, the apparent further increase of the 136.5-keV γ-production cross section seems an artificial artifact due probably to a contamination component; also, the last three points from Fig. 4(b) are affected by high uncertainties. The same remark is also valid for the 352.4-keV transition: the last 4 points of that γ production cross section, corresponding to E$_n$ ≥7 MeV, are affected by large uncertainties and therefore they should be disregarded. Indeed, the apparent increase of the cross section in that energy region constitutes an unphysical feature that should not be considered when the comparison with the theoretical calculations is performed. The default TALYS and EMPIRE calculations seem to reproduce the first bump of the two cross sections observed in Ref. [8] but in the range E$_n$=2.5-9 MeV they are very close to our result.

In order to get additional insight in the shape difference between our 122.1-keV γ-production cross section and the one reported in Ref. [8] we revisited the data collected during a previous measurement using a ^{nat}Fe sample [3]. The old experiment was performed with GAINS at GELINA a few years ago employing only four HPGe detectors. Unfortunately, due to the fact that our main goal at that time was to study the ^{56}Fe(n, $n\gamma$)^{56}Fe reaction where the γ-ray energies are significantly higher, the electronic threshold we set in that experiment did not allow us to determine accurately the detector efficiencies at E_γ=122.1 keV. Therefore, although the 122.1-keV peak is visible in the spectra, the absolute cross sections could not be determined. Nevertheless, we could determine the shape of the γ-production cross section that is compared in Fig. 5 with the present measurement and with the result from Ref. [8]. The fact that the shape seems to overlap better with the present measurement rises our confidence (also in this case the comparison above E$_n$ ≈10 MeV should be disregarded as the values have large uncertainties).

Our γ-energy resolution did not allow the separation of the 990.1-keV γ ray emitted from the 1356.8-keV level from the 992.7-keV γ ray decaying from the 1007.1-keV level. Therefore the production cross section displayed in Fig. 4(g) represents the sum of the two transitions and the comparison is also made with the sum of the two theoretically calculated γ-production cross sections.

Based on the strange shape and very high values of the 1061.6-keV γ-production cross section from the (n, n') channel, the authors of Ref. [8] speculated that a transition with the same energy was also excited in the ^{57}Fe(n, p)^{54}Cr reaction. This hypothesis was not con-

firmed by other experiments investigating the structure of ^{54}Cr. Our γ-production cross section for the 1061.6-keV transition shown in Fig. 4(h) is indeed smaller and has a different shape compared to the one from Ref. [8].

2. *Modeling of the γ-production cross sections*

The two theoretical calculations performed with the TALYS and EMPIRE codes using default parameters shown in Fig. 4 are pretty similar mainly because both codes use the same global optical potential for neutrons developed by Koning and Delaroche (RIPL-2405 [27]). The differences may be caused by the different treatment of the widths fluctuation, of the preequilibrium emission exciton model, level densities, etc. However, there is a significant difference related to the way the two codes treat the γ decay of the levels for which no branching ratios are provided. In such cases EMPIRE considers transitions directly to the ground state, while TALYS makes educated assumptions regarding possible transitions. In ^{57}Fe there is a level with the excitation energy of 1139.9 keV and no branching ratio whose existence is questioned by the structure evaluators [6] (see Fig. 2). In the Level segment of RIPL-3 [21] used by EMPIRE the spin and parity of this level is $J^\pi = 3/2^+$. In the structure file used by TALYS it has $J^\pi = 9/2^-$ and it is considered by the code to decay through two equally-probable transitions towards the 706.4- and the 136.6-keV, $5/2^-$ states. This explains the significant difference between the predictions of the two codes for the 692-keV γ-production cross section. We consider that TALYS assumptions are not sustainable: the two γ transitions of 433.5 and 1003.4 keV from the 1139.9-keV level should have, according to the same TALYS calculation, cross sections reaching ≈0.05 b for E_n ≈10 MeV, a strength comparable with the one of the 366.8-keV γ ray that we measured. However, we did not observe in our spectra such peaks at 433.5 or 1003.4 keV.

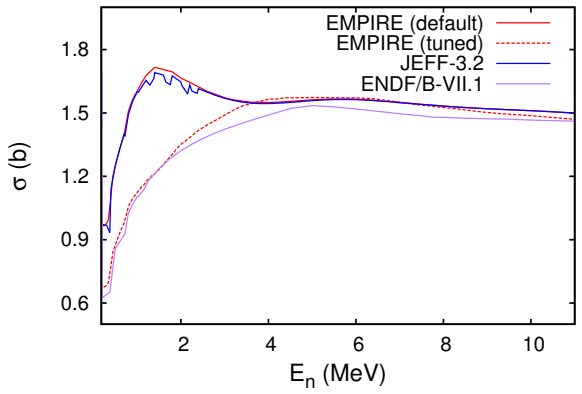

FIG. 6: (Color online) Neutron nonelastic cross section on ^{57}Fe calculated with EMPIRE, compared to the values from the evaluated libraries JEFF-3.2 and ENDF/B-VII.1.

In general, the model calculations follow the shape of the experimental data, except for the significant overestimation below incident energies around 3 MeV. In order to understand the origin of these discrepancies, a full analysis of all available experimental data from the experimental database EXFOR [28] and most recent evaluations have been performed using the EMPIRE code.

The nonelastic cross section calculated using EMPIRE is compared in Fig. 6 to the evaluations from The Evaluated Nuclear Data File, ENDF/B-VII.1 [29] and The Joint Evaluated Fission and Fusion File, JEFF-3.2 [30] (we mention that in the energy range 150 keV - 5 MeV the nonelastic and inelastic cross sections are almost identical). The first thing to be noticed is that the EMPIRE default calculation coincides with the JEFF-3.2 evaluation. Indeed, JEFF-3.2 is based on TALYS calculations and that both TALYS and EMPIRE are using for iron isotopes as default a spherical optical model with the Koning Delaroche regional optical potential [27]. Considering that the nonelastic cross section depends exclusively on the optical model, one can understand why the two codes produce identical results.

The second aspect shown by Fig. 6 is that EMPIRE and JEFF-3.2 overestimate ENDF/B-VII.1 in the same energy range where the present experimental $(n, n\gamma)$ data are overestimated by the theoretical predictions. Accurate description of the measured cross section in this energy region requires an optical model potential that depends on the incident partial wave [32]. There is no global optical potential describing properly the neutron interaction with the nuclei in the iron region. For example, coupled channels calculations performed with the dedicated optical model potential RIPL-615 [33] produced similar results at low incident energies as those using the regional spherical optical potential RIPL-2405 [27]. For the purpose of this paper, we decided to describe the direct interaction with the spherical optical model (using the optical potential RIPL-2405) and the distorted wave Born approximation, and to adjust the resulted nonelastic cross section to fit the measured $(n, n\gamma)$ cross sections at low energies. For the other reaction mechanisms we used the pre-equilibrium exciton model and the Hauser-Feshbach statistical model [34] with the width fluctuation correction proposed by Hoffman-Richert-Tepel-Weidenmüller (HRTW) [35]. Gilbert-Cameron composite formula was employed for the level densities and the modified Lorentzian model (MLO1) was selected for the γ strength functions. The model parameters were retrieved from RIPL-3 [21].

There is a significant difference between the treatment of the γ decay of the levels in the discrete and in the continuum region. The γ decay of a discrete level is fully defined by the level scheme which provides energies, spins, parities, branching ratios, and internal conversion coefficients obtained mainly on an experimental basis. In continuum, the decay of a level with a given spin and parity within an energy bin populates lower energy bins and discrete levels according to the γ strength functions and

the spin and parity selection rules. As the description of γ transitions in the discrete spectrum is much more accurate than of the γ cascade from continuum, it is desirable to consider the number of discrete levels N_d as large as possible. Unfortunately, this number is limited by the completeness of the decay scheme. Most reaction codes derive the parameters of the level densities from the fit of the cumulative number of the low lying levels. If the matching between the discrete and continuum spectrum is in a region with missing levels, the level density is significantly affected. For the present calculations we used N_d=25 levels to have a right behavior of the level density, hence of the inelastic and other competing channels cross sections.

Figure 7 displays the production cross sections of the 122.1- and 692.0-keV photons calculated with EMPIRE using N_d=25 levels (full curve) and N_d=100 levels (dashed curve). For a better understanding of the impact of the number of discrete levels on the population cross section, we mention that at low energies, just above the threshold, the contribution of the side feeding dominates while at high energies the γ cascade from continuum is more important. In the latter the impact of the level density description is the dominant factor, a higher level density resulting in larger calculated cross sections. In between, the contributions of the γ decay of the discrete states play the most significant role. The $(n, n\gamma)$ cross sections measured in the present experiment could be divided in two categories: with the maximum at intermediate energies and with the maximum around E_n=8 MeV, just below the $(n, 2n)$ threshold. From the shape of these cross sections one can deduce which population mechanism is more important for each level: for the 136.5-, 1007.1- and the 1197.8-keV levels the γ cascade from continuum (transitions from levels with high excitation energies) dominates, while for the 366.8-, 706.4- and the 1356.8-keV states the γ cascade initiated from discrete or continuum levels with lower excitation energies is more significant. This explains the different impact of increasing the number of discrete levels on the 122.1- and 692.0-keV transitions shown by Fig. 7. In the case of the 122.1-keV transition, the decrease at high energies is caused by the missing levels, and by the level density lowered because of the automatic fit of the cumulative number of levels. In case of the 692.0-keV γ ray, the increase of the population cross section at intermediate energies is due to the higher number of transitions in the discrete spectrum.

In conclusion, the differences between the default EMPIRE calculations and our measured data have three causes: deficiencies in the reaction modeling, in the discrete level scheme, and in the experimental data. Our next goal was to tune the EMPIRE calculations in order to reproduce as well as possible the available measured data and to use the consistency of the model calculation to derive the production cross section of the 14.4-keV γ ray which could not be measured. Two adjustments were applied:

(i) The nonelastic cross section was adjusted with an energy dependent factor varying from 0.7 at 0.1 MeV to 1 at 3 MeV in order to correct the optical model prediction. We remind that this is a resonance region which cannot be properly described by optical and statistical models. The adjustment factor was selected to improve the agreement between the calculated and the measured production cross sections for the 122.1-keV γ ray (which represents the highest contribution to the population of the first excited level) in this energy range. By imposing this experimental constraint, the resulted nonelastic cross section gets closer to the ENDF/B-VII.1 evaluation (see the dashed curve in Fig. 6). The correction of the nonelastic cross section improves the agreement between the EMPIRE calculations and our measured data at low energies. Usually, any adjustment of the nonelastic cross section requires a compensating adjustment of the elastic contribution to preserve the total cross section. In this case, the consequence of the nonelastic cross section reduction is that the calculated total cross section represents a better average of the resonant experimental total cross section in the mentioned energy range.

(ii) Some of the level population cross sections have been adjusted to compensate the impossibility of considering a large number of transitions between discrete levels and at the same time to start the continuum in an energy range without missing levels. This adjustment might also compensate for wrongly assigned spins, parities and branching ratios in the level scheme. In most of the cases, the agreement between the experimental data and the model prediction (the full curves in Fig. 8) improves significantly. We underline that any change of the partial inelastic cross sections is automatically compensated by a change of the competing channels, mainly the compound elastic cross section, so that the compound nucleus cross section is conserved.

Figure 8 compares these tuned EMPIRE calculations with our experimental results. The dashed lines represent the calculations after the correction of the nonelastic cross section but before adjusting the level population cross sections while the continuous lines represent the best-tuned calculations.

We will further analyze each transition starting with those decaying from the highest levels. The double-humped shape of the E_γ=650.4 keV calculated production cross section and the comparison with the measured data [Fig. 8(j), the dashed curve] suggest a good description of the side-feeding (represented by the first hump), a good description of the γ cascade from continuum (represented by the second hump), but a too small contribution or no contribution at all from the γ transitions among discrete levels (indicated by the dip of the excitation function in the energy range 2.4 - 10 MeV). Indeed,

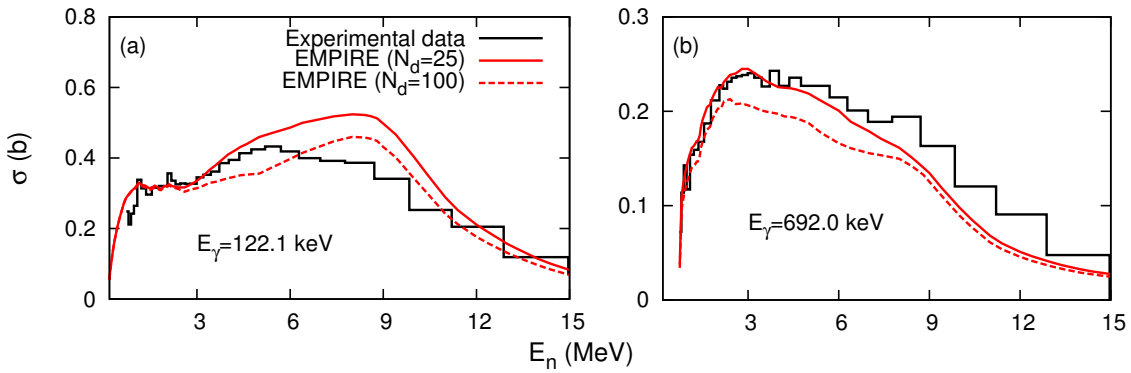

FIG. 7: (Color online) The impact of the number of discrete levels on the EMPIRE calculated production cross sections of the (a) 122.1- and (b) 692.0-keV γ transitions. The continuous lines correspond to N_d=25 levels while the dashed ones are obtained using N_d=100.

according to the Levels Segment in RIPL-3, none of the first N_d=25 levels decays to the 1356.8-keV level. In fact, in the entire scheme, there are only four levels feeding this state (at 3.18, 3.32, 4.13 and 4.92 MeV) and their contributions are small. As there are no arguments to include additional decays in the level scheme, we increased the partial inelastic compound nucleus cross section in order to reproduce the measured data (see the full curve from Fig. 8).

The 650.4-keV γ ray represents the most important transition among discrete states populating the fourth excited level at 706.4 keV, and therefore the 692.0-keV calculated γ-production cross section underestimates the measured data mostly in the same energy range. According to the experimental data, the calculated population of the 706.4-keV level is too small on the entire energy range suggesting either a too small side feeding or, more likely, missing decays of levels just above.

The 1061.6-keV calculated γ-production cross section describes reasonably well the measured data. One can notice a slight overestimation in the energy range 2-3 MeV caused either by a too high side-feeding or by too high branching ratios, and an overestimation around 8 MeV caused by an overestimated contribution of the γ cascade from continuum. We mention that by increasing the number of discrete levels, the structure around 4 MeV is better reproduced.

The 898.4-keV γ-production cross section calculated with EMPIRE follows well the trend of the measured data.

The calculated 366.8-keV γ-production cross section follows the trend of the measured data, but underestimates them starting from energies lower than the excitation energy of the last discrete level. This suggests that some decays which populate this level are missing or have too low intensities. Adjusting the population of the third excited level in this region to fit these data is not enough to describe also the experimental data for the 352.4-keV transition which remains underestimated.

Finally, the 122.1-keV transition represents the most important contribution to the population of the first excited level coming from a discrete state. It is important to stress out the insignificant impact on the population of this level of the changes we did on the population of the levels above. The model calculation overestimates the experimental data above E_n=5 MeV. This happens also for the 136-keV transition, but it is less visible because of the dispersion of our experimental data in this energy range. The most probable cause of this disagreement is a too strong contribution of the γ cascade from continuum to the population of the second excited level. Other formulations and parameters of the γ strength function and of the level density function do not improve the agreement.

B. Branching ratios in ^{57}Fe

TABLE I: Branching ratios in ^{57}Fe. The present results are compared with values from the evaluated level scheme [6].

E_L (keV)	E_γ (keV)	Branching ratio		
		ENSDF ([6])	Present result	
			Unweighted avg.	Weighted avg.
136.5	122.1	100(10)	100	100
	136.5	12.0(12)	12.32(17)	12.29(21)
366.8	352.4	100(11)	100	100
	366.8	17.7(20)	14.2(3)	14.3(2)

In two cases, two γ rays decaying from a level were detected, allowing calculation of the branching ratio.

In order to do so we determined the ratio of the two cross sections for each value of the incident neutron energy. The resulting ratios were then averaged using a weighted and an unweighed averaging procedure while excluding the discrepant values. Table I compares our results with the evaluated values from Ref. [6]. For the

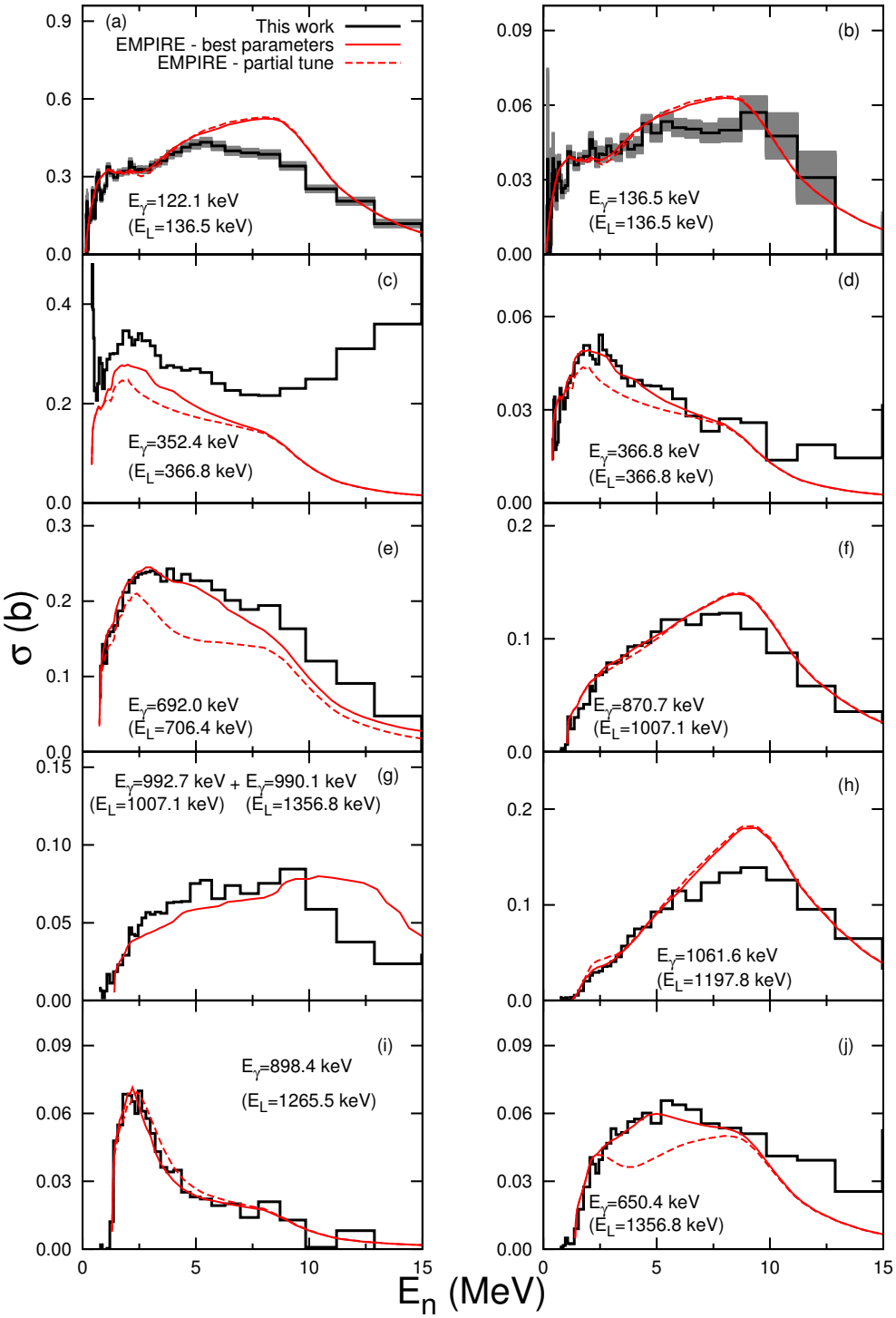

FIG. 8: (Color online) Production cross sections for the γ rays emitted following the ^{57}Fe(n, $n\gamma$) reaction. Comparison of the tuned EMPIRE calculations with our experimental results. The dashed lines display the calculation results after adjusting the nonelastic cross section but before adjusting the level population cross sections while the continuous lines represent the best-tuned calculations. See the text for details.

transitions starting from the 136.5-keV level our branching ratios are in agreement with the previous values while the uncertainty is much smaller. For the transitions starting from the 366.8-keV level the difference between our result and the previously evaluated branching ratios is just at the limit of the uncertainty range.

Fig. 4(f and g) displays also the production cross sections of two γ rays decaying from the 1007.1-keV level.

TABLE II: Level cross section formulas and ranges. The coefficients of the γ-production cross sections $\sigma_\gamma(E_n)$ were calculated using branching ratios and conversion coefficients from Ref. [6].

	Formula	Range (keV)
$\sigma_L^{136.5}(E_n) =$	$1.160(103)\sigma_\gamma^{122.1}(E_n) - 0.092(11)\sigma_\gamma^{352.4}(E_n) - \sigma_\gamma^{870.7}(E_n)$	138.89 - 2011.65
$\sigma_L^{366.8}(E_n) =$	$1.269(112)\sigma_\gamma^{352.4}(E_n) - 0.017(3)\sigma_\gamma^{692.0}(E_n)$	373.26 - 1656.09
	$-0.047(32)\sigma_\gamma^{870.7}(E_n) - \sigma_\gamma^{898.4}(E_n) - 0.43(7)\sigma_\gamma^{650.4}(E_n)$	
$\sigma_L^{703.4}(E_n) =$	$1.184(113)\sigma_\gamma^{692.0}(E_n) - \sigma_\gamma^{1061.6}(E_n) - \sigma_\gamma^{650.4}(E_n)$	718.93 - 1656.09

Unfortunately, as already mentioned, the peak corresponding to the 992.7-keV transition overlaps in our spectra with the one of the 990.1-keV γ ray decaying from the 1356.8-keV excited level. Due to this fact we could not determine also the branching ratio of the 992.7-keV γ ray.

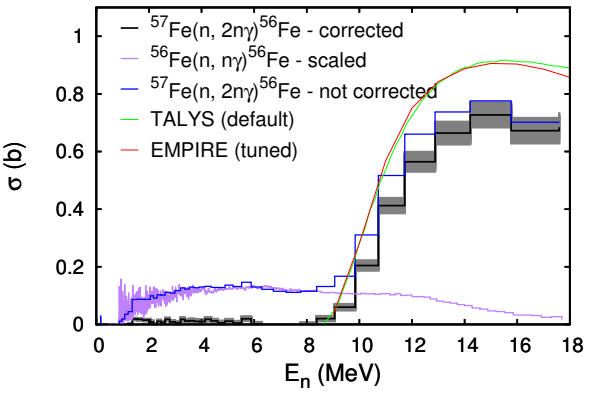

FIG. 9: (Color online) 846.8-keV γ production cross sections from the ^{57}Fe(n, $2n$)^{56}Fe reaction. The blue curve displays the raw cross section we measured. The purple line is the ^{56}Fe(n, $n\gamma$) cross section from Ref. [3] scaled for the relative abundance of ^{56}Fe and ^{57}Fe in our target. The black line represents our final result (together with the gray uncertainty band) compared with the TALYS default calculation displayed in green and the tuned EMPIRE calculations in red.

C. The 846.8-keV γ-production cross section from the ^{57}Fe(n, $2n$)^{56}Fe reaction

Due to the particular importance of this transition, we performed a dedicated analysis to determine the γ-production cross section for the 846.8-keV transition excited in the ^{57}Fe(n, $2n$)^{56}Fe reaction. As the natural abundance of ^{57}Fe is 2.12(3)% [4], the total production cross section for the 846.8-keV γ ray on ^{nat}Fe contains, above E$_n$=8.64 MeV, a component from the ^{57}Fe(n, $2n$)^{56}Fe reaction. Although this is not a very high contribution (see also the discussion from Ref. [3]), the current data represents an opportunity to estimate it.

The blue line from Fig. 9 represents the 846.8-keV γ-production cross section from our sample. The component below E$_n$=8.64 MeV is due to the (n, $n\gamma$) reaction on ^{56}Fe (the ^{56}Fe content in our sample was 9.15(30)%). Indeed, by scaling the 846.8-keV γ-production cross section reported in Ref. [3] with the relative abundances of ^{56}Fe and ^{57}Fe in our sample (9.15 / 90.50), we obtained the purple line from Fig. 9. After a proper rebinding we subtracted these two curves obtaining the black line. This component represents therefore the 846.8-keV γ-production cross section in the ^{57}Fe(n, $2n$)^{56}Fe reaction. It is compared in Fig. 9 with a theoretical calculation using the default parameters in TALYS and with the tuned EMPIRE calculations which overlap almost completely.

D. Level cross sections

For three excited states in ^{57}Fe (E$_L$=136.5, 366.8 and 703.4 keV) we observed sufficient feeding and decaying transitions to be able to build the level cross sections $\sigma_L(E_n)$ using the equations from Table II. The experimental results are compared in Fig. 10 with the evaluated cross sections from ENDF/B-VII.1 [29] and JEFF-3.2 [30] but also with the theoretical calculations performed with EMPIRE using the tuned parameters. We note that the JEFF-3.2 evaluation overlaps perfectly with the default TALYS calculations and the ENDF/B-VII.1 evaluation overlaps with the Japanese Evaluated Nuclear Data Library, JENDL-4.0 [31].

The validity ranges from the last column of Table II are based on the evaluated level scheme of ^{57}Fe [6]: in each case the lower limit is defined by the smallest neutron energy required to excite the level of interest. The higher limit represents the neutron energy required to excite a higher-lying state that decays to the level of interest through a γ transition that we could not detect. Below this range the level cross section is by definition zero while above it the values we provide represent only higher limits of the real level cross sections. This is obvious in Fig. 10 where, above E$_n$≈2 MeV the experimental curves do not follow the natural decrease shown by the theoretical predictions and the evaluations.

Moreover, we note also that, at low neutron energies, the disagreement between JEFF-3.2 (overlapping with the default TALYS calculation) and our experimental result is significant. This behavior was, however, already expected from the shape shown by the calculated γ-production cross sections, displayed in Fig. 4: In many

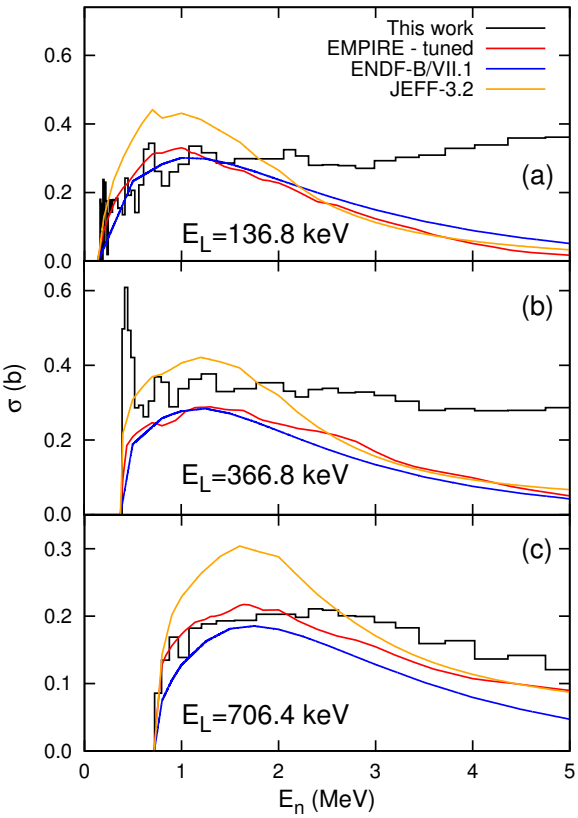

FIG. 10: (Color online) Level cross sections in the ^{57}Fe(n, n') reaction. The ranges where our values are strictly correct are listed in Table. II. Above the specified ranges our values represent higher limits of the level cross sections. The experimental results are compared with the evaluated cross sections from ENDF/B-VII.1 and JEFF-3.2 but also with the tuned EMPIRE calculations. We note that the JEFF-3.2 evaluation overlaps perfectly with the default TALYS calculations (not shown here) and the ENDF/B-VII.1 evaluation overlaps with JENDL-4.0 (also not shown).

cases, the TALYS calculations show a bump in the neutron energy range between 1 and 2 MeV. This feature, although visible in the ORNL data [8] is not confirmed by our results.

Finally, the most important observation for the aim of this paper is the very good agreement above the resonance region between the first level population cross section predicted by EMPIRE using the present measured data as constraint and those from ENDF/B-VII.1 and JENDL-4.0 libraries.

E. Theoretical deduction of total inelastic cross section using EMPIRE

The most difficult part of the present analysis is the derivation of the total inelastic cross section by combining the EMPIRE generated 14.4-keV γ-production cross section with the other experimentally determined cross sections of the γ rays that populate the ground state.

Based on the level scheme (see also Fig. 2) and taking into account the branching ratios and the conversion coefficients from Ref. [6], the equation used to calculate the total inelastic cross section was:

$$\begin{aligned}\sigma_{inel}(E_n) =& 9.56(26)\sigma_\gamma^{14.4}(E_n)+ \\ & 1.137(15)\sigma_\gamma^{136.5}(E_n)+ \\ & 1(0)\sigma_\gamma^{366.8}(E_n)+ \\ & 0.057(24)\sigma_\gamma^{692.0}(E_n)+ \\ & 0.027(7)\sigma_\gamma^{898.4}(E_n)\end{aligned} \quad (3)$$

We emphasize again that in Eq. (3) the first term is theoretically calculated while the others are purely experimental. The validity range of the total inelastic cross section extends from the threshold for the neutron inelastic scattering (E_n=14.7 keV) up to the threshold for exciting a level that decays to the ground state and from which we could not detect any γ ray (this level lies at 1627.3 keV [6] and the neutron energy threshold to excite it is E_n=1655.8 keV). However, in case of the low neutron energies, due to small values of the neutron flux from GELINA below E_n $\approx$300 keV combined with the relatively small thickness of our ^{57}Fe sample, the statistical uncertainties of our cross sections are very large. Therefore we consider that the validity of the cross sections we report in the present paper does not extend below 300 keV.

Figure 11 displays the total inelastic cross section calculated using Eq. (3) compared with the tuned EMPIRE calculation. The main contributing γ-production cross sections are also displayed, scaled with the factors from Eq. (3). An uncertainty of 10% was attributed to the calculated γ-production cross section for the 14.4-keV transition based on the level of overlap between the EMPIRE calculations and the experimental results.

The first observation is that the total inelastic cross section is dominated by the contribution coming from the 14.4-keV transition. Although the γ cross section is not very large in this case, the total transition is large due to the very large conversion coefficient, α=8.56(26) [6]. Indeed, most of the neutron inelastic strength is collected through the first excited state. On the other hand, at neutron energies above 3 MeV, it is interesting to note that in case of ^{57}Fe there is an important difference between the 14.4-keV γ-production cross section and the total inelastic cross section calculated by EMPIRE. This is mainly due to the contributions from continuum that are significant in the neutron energy region above 3 MeV.

The total inelastic cross section generated by this interplay between our experimental data and the dedicated, fine-tuned theoretical calculations is not a purely experimental result and for this reason it has an uncertainty of the level of 10%. However these values represent the best total inelastic cross sections compatible with our experimental results.

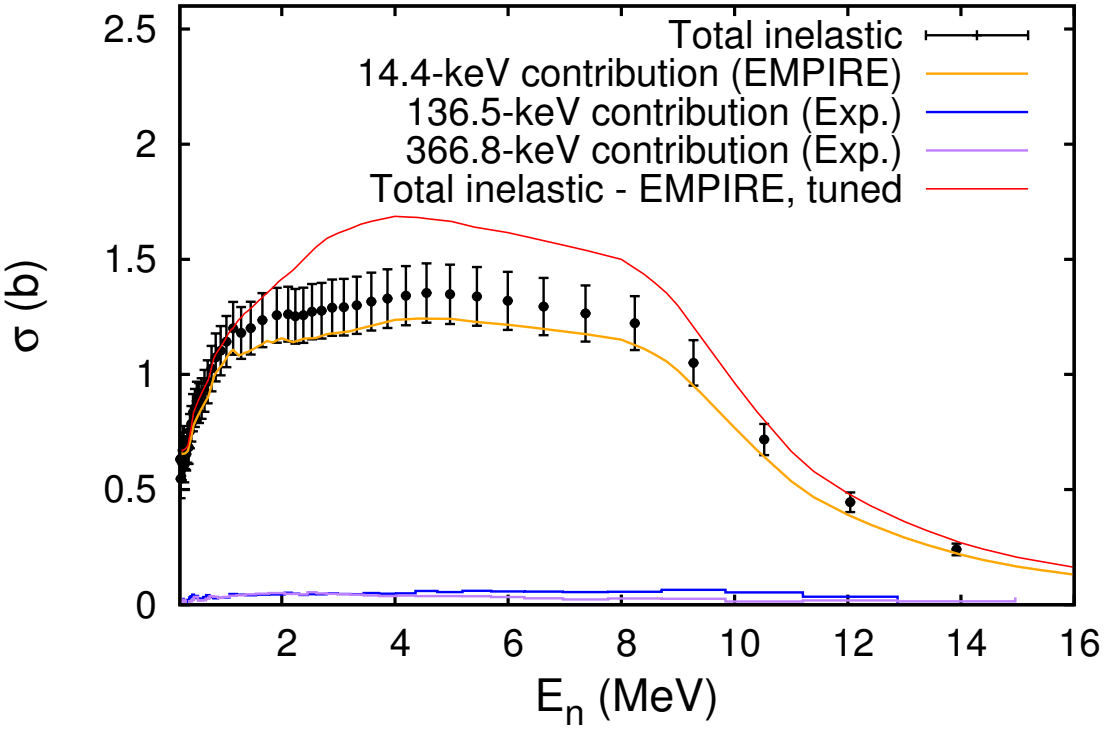

FIG. 11: (Color online) Total inelastic cross section for the ^{57}Fe(n, n') reaction (black points), calculated based on the theoretically determined contribution of the 14.4-keV γ-production cross section (orange line) and the experimental results for the 136.5- (blue line), 366.8- (violet line), 692.0- and 898.4-keV γ-production cross sections. The red line shows the total inelastic cross section calculated by EMPIRE using the tuned parameters.

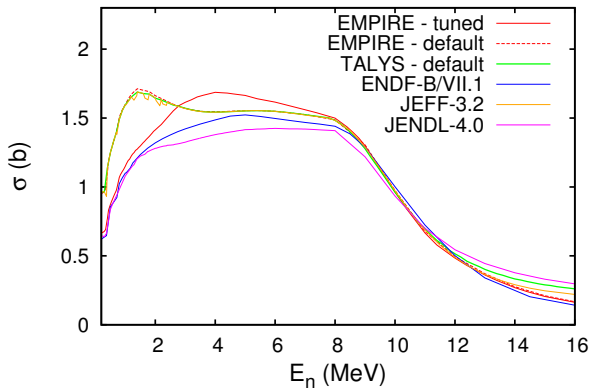

FIG. 12: (Color online) Theoretically calculated total inelastic cross section for the ^{57}Fe(n, n') reaction compared to various evaluations. Both default EMPIRE and TALYS calculations overlap almost completely with the JEFF-3.2 evaluation.

Figure 12 compares the ^{57}Fe total neutron inelastic cross section calculated using various theoretical approaches (TALYS with default parameters, EMPIRE with default parameters, EMPIRE with tuned parameters) with the evaluated libraries (ENDF-B/VII.1, JEFF-3.2 and JENDL-4.0). We note also in this case that the default EMPIRE and TALYS calculations overlap almost perfectly with JEFF-3.2.

Further, in Fig. 12 one can observe the significant difference between the initial model prediction of the inelastic cross section and the final inelastic cross section adjusted to describe the present $(n, n'\gamma)$ measurements. Even if its absolute value might have a rather large uncertainty, the shape of the final cross section became typical for the inelastic process and similar to those of the ENDF-B/VII.1 and JENDL-4.0 evaluations. This result shows once again the importance of the experimental data in constraining the model calculations, especially for those nuclei and energy ranges where the optical potentials fail to describe properly the nuclear interaction.

F. Concluding remarks

In conclusion, we measured the production cross sections for 10 γ rays excited in the ^{57}Fe(n, n')^{57}Fe reaction using a large volume enriched sample. Significant discrepancies were found compared to the previous measurement performed in the eighties at ORNL.

The first γ transition from ^{57}Fe (E$_\gamma$=14.4 keV) could

not be detected with our HPGe array due to the background level at low γ energies and therefore an interplay between the experimental data and theoretical calculations was used to generate the total inelastic cross section.

No γ transition decaying from the questionable 1139.9-keV level [6] was detected in our experiment. In particular, the 433.5- and 1003.4-keV transitions assumed by the default TALYS structure file were not confirmed.

Considering the scarcity of the experimental information on the neutron induced reactions on ^{57}Fe and the difficulties in deriving a proper optical potential to describe these interactions, the present measurement represents an important constraint for the nuclear data evaluation. The adjustment of the calculated nonelastic cross section used to describe the measured $(n, n\gamma)$ cross sections improved the overall agreement with the existing experimental data and with the latest evaluations. Even if ^{57}Fe is a minor isotope, an accurate evaluation of its neutron reaction data is needed to extract information on ^{56}Fe from the experimental data for natural iron. This subject is important for ongoing projects such as CHANDA and CIELO.

Several options are possible in order to directly determine the cross sections for the first transition: the detection of the conversion electrons, the evacuation of the area around the sample in order to limit the background induced by neutrons scattering on air (possibly by using an additional beam pipe under vacuum), the use of planar HPGe detectors. Although each of these possibilities presents specific challenges, advantages and disadvantages, they are all currently under investigation.

Acknowledgments

The authors thank the team of operators of the GELINA facility for the preparation of the neutron beam and to the technical staff of JRC-Geel for their support during the data taking campaign. The isotope used in this research were supplied by the United States Department of Energy Office of Science by the Isotope Program in the Office of Nuclear Physics. This work was partially supported by the European Commission through the ANDES (EURATOM Contract number FP7-249671), EUFRAT (EURATOM Contract number FP7-211499), and CHANDA (EURATOM contract number FP7-605203) projects.

[1] OECD, Nuclear Energy Agency, Collaborative International Evaluated Library Organisation (CIELO) Pilot Project, WPEC Subgroup 40 (SG40), https://www.oecd-nea.org/science/wpec/sg40-cielo
[2] https://www.oecd-nea.org/dbdata/hprl
[3] A. Negret, C. Borcea, Ph. Dessagne, M. Kerveno, A. Olacel, A.J.M. Plompen, and M. Stanoiu, Phys. Rev. C**90**, 034602 (2014).
[4] J. Meija *et al.*, Pure and Appl. Chem. **88**, 293-306 (2016).
[5] H. Junde, H. Su, and Y. Dong, Nucl. Data Sheets **112**, 1513 (2011).
[6] M.R. Bhat, Nucl. Data Sheets **85**, 415 (1998).
[7] Y. Dong and H. Junde, Nucl. Data Sheets **121**, 1 (2014).
[8] Z.W. Bell, J.K. Dickens, D.C. Larson, and J.H. Todd, Nucl. Sci. Eng. **84**, 12 (1983).
[9] C. Rouki, P. Archier, C. Borcea, C. De Saint Jean, J.C. Drohe, S. Kopecky, A. Moens, N. Nankov, A. Negret, G. Noguere, A.J.M. Plompen, and M. Stanoiu, Nucl. Instrum. Methods Phys. Research A**672**, 82 (2012).
[10] A. Negret, C. Borcea, D. Bucurescu, D. Deleanu, Ph. Dessagne, D. Filipescu, D. Ghita, T. Glodariu, M. Kerveno, N. Marginean, R. Marginean, C. Mihai, S. Pascu, A.J.M. Plompen, T. Sava, and L. Stroe, Phys. Rev. C**88**, 034604 (2013).
[11] A. Olacel, C. Borcea, Ph. Dessagne, M. Kerveno, A. Negret, and A.J.M. Plompen, Phys. Rev. C**90**, 034603 (2014).
[12] D. Ene, C. Borcea, S. Kopecky, W. Mondelaers, A. Negret, and A.J.M. Plompen, Nucl. Instrum. Meth. Phys. Research A**618**, 54 (2010).
[13] D. Deleanu, C. Borcea, Ph. Dessagne, M. Kerveno, A. Negret, A.J.M Plompen, and J.C. Thiry, Nucl. Instrum. Methods Phys. Research A**624**, 130 (2010).
[14] A. Plompen, N. Nankov, C. Rouki, M. Stanoiu, C. Borcea, D. Deleanu, A. Negret, Ph. Dessagne, M. Kerveno, G. Rudolf, J.C. Thiry, M. Mosconi, and R. Nolte, J. Korean Phys. Soc.**59**, 1581 (2011).
[15] D. Tronc, J.M. Salomé, and K. Böckhoff, Nucl. Instrum. Meth. Phys. Research A**228**, 217 (1985).
[16] L.C. Mihailescu, L. Olah, C. Borcea, and A.J.M Plompen, Nucl. Instrum. Meth. Phys. Research A**531**, 375 (2004).
[17] A.D. Carlson, V.G. Pronyaev, D.L. Smith, N.M. Larson, Z. Chen, G.M. Hale, F.-J. Hambsch, E.V. Gai, S.-Y. Oh, S.A. Badikov, T. Kawano, H.M. Hofmann, H. Vonach, and S. Tagesen, Nucl. Data Sheets **110**, 3215 (2009).
[18] M. Herman, R. Capote, B.V. Carlson, P. Obložinský, M. Sin, A. Trkov, H. Wienke, and V. Zerkin, Nucl. Data Sheets **108**, 2655 (2007).
[19] M. Herman, R. Capote, M. Sin, A. Trkov, B.V. Carlson, P. Oblozinsky, C.M. Mattoon, H. Wienkey, S. Hoblit Young-Sik Cho, G.P.A. Nobre, V. Plujko, and V. Zerkin, EMPIRE-3.2 (MALTA) User's Manual, report INDC(NDS)-0603 of the International Atomic Energy Agency, Vienna (2013)
[20] A.J. Koning, S. Hilaire and M.C. Duijvestijn, in *Proceedings of the International Conference on Nuclear Data for Science and Technology - ND2007, April 22-27, 2007, Nice, France*, editted by O. Bersillon, F. Gunsing, E. Bauge, R. Jacqmin, and S. Leray, EDP Sciences, 2008, p. 211.
[21] R. Capote, M. Herman, P. Oblozinsky, P.G. Young, S. Goriely, T. Belgya, A.V. Ignatyuk, A.J. Koning, S. Hilaire, V.A. Plujko, M. Avrigeanu, O. Bersillon,

M.B. Chadwick, T. Fukahori, Zhigang Ge, Yinlu Han, S. Kailas, J. Kopecky, V.M. Maslov, G. Reffo, M. Sin, E.Sh. Soukhovitskii, and P. Talou, Nucl. Data Sheets **110**, 3107 (2009).

[22] T. Kawano, P. Talou, and H.A. Weidenmüller, Phys. Rev. C**92**, 044617 (2015).

[23] T. Kawano, R. Capote, S. Hilaire, and P. Chau Huu-Tai, Phys. Rev. C**94**, 014612(2016).

[24] W.E. Kinney and J.W. McConnell, High resolution neutron scattering experiments at ORELA, Symposium Lowell 1976, EXFOR 10571002.

[25] M.B. Chadwick, E. Dupont, E. Bauge, *et al*, Nucl. Data Sheets **118**, 1 (2014).

[26] R. Capote and A. Trkov (coordinators), IAEA CIELO Data Development Project within the International Pilot Project of the OECD/NEA, `https://www-nds.iaea.org/CIELO/`

[27] A.J. Koning and J.P. Delaroche, Nucl. Phys. A**713**, 231 (2003).

[28] N. Otuka, E. Dupont, V. Semkova, B. Pritychenko, A.I. Blokhin, M. Aikawa, S. Babykina, M. Bossant, G. Chen, S. Dunaeva, R.A. Forrest, T. Fukahori, N. Furutachi, S. Ganesan, Z. Ge, O.O. Gritzay, M. Herman, S. Hlavač, K. Katō, B. Lalremruata, Y.O. Lee, A. Makinaga, K. Matsumoto, M. Mikhaylyukova, G. Pikulina, V.G. Pronyaev, A. Saxena, O. Schwerer, S.P. Simakov, N. Soppera, R. Suzuki, S. Takács, X. Tao, S. Taova, F. Tárkányi, V.V. Varlamov, J. Wang, S.C. Yang, V. Zerkin, Y. Zhuang, Nucl. Data Sheets **120**, 272 (2014).

[29] M.B. Chadwick, M. Herman, P. Obložinský, M.E. Dunn, Y. Danon, A.C. Kahler, D.L. Smith, B. Pritychenko, G. Arbanas, R. Arcilla, R. Brewer, D.A. Brown, R. Capote, A.D. Carlson, Y.S. Cho, H. Derrien, K. Guber, G.M. Hale, S. Hoblit, S. Holloway, T.D. Johnson, T. Kawano, B.C. Kiedrowski, H. Kim, S. Kunieda, N.M. Larson, L. Leal, J.P. Lestone, R.C. Little, E.A. McCutchan, R.E. MacFarlane, M. MacInnes, C.M. Mattoon, R.D. McKnight, S.F. Mughabghab, G.P.A. Nobre, G. Palmiotti, A. Palumbo, M.T. Pigni, V.G. Pronyaev, R.O. Sayer, A.A. Sonzogni, N.C. Summers, P. Talou, I.J. Thompson, A. Trkov, R.L. Vogt, S.C. van der Marck, A. Wallner, M.C. White, D. Wiarda, and P.G. Young, Nucl. Data Sheets **112**, 2887 (2011).

[30] JEFF Scientific Working group, Nuclear Energy Agency Data Bank, Joint Evaluated Fission and Fusion File (JEFF) release 3.2, OECD, March 5 (2014), `https://www.oecd-nea.org/dbforms/data/eva/evatapes/jeff_32`

[31] K. Shibata, O. Iwamoto, T. Nakagawa, N. Iwamoto, A. Ichihara, S. Kunieda, S. Chiba, K. Furutaka, N. Otuka, T. Ohsawa, T. Murata, H. Matsunobu, A. Zukeran, S. Kamada, and J. Katakura, J. Nucl. Sci. Tech. **48**, 1 (2011).

[32] T. Kawano and F. Fröhner, Nucl. Sci. Eng. **127**, 130 (1997).

[33] Rui Li, Weili Sun, E.Sh. Soukhovitskii, J.M. Quesada, and R. Capote, Phys. Rev. C**87**, 054611 (2013).

[34] W. Hauser and H. Feshbach, Phys. Rev. C**87**, 366 (1952).

[35] H.M. Hoffmann, J. Richert, J.W. Tepel and H.A. Weidenmüller, Ann. Phys. (N.Y.) **90**, 403 (1975).